AIAA JOURNAL
Vol. 39, No. 4, April 2001

Three-Dimensional Thermochemical Nonequilibrium Viscous Flow over Blunt Bodies with Catalytic Surface

S. Peigin* and V. Kazakov†
Tomsk University, 634050 GSP-14, Tomsk, Russia
and
M.-C. Druguet,‡ S. Séror,§ and D. E. Zeitoun¶
Université de Provence, 13453 Marseille Cedex 13, France

The hypersonic thermochemical nonequilibrium airflow over the catalytic surface of a blunt body moving at attack and slip angles along a prescribed aerodynamic reentry trajectory is considered. The thin viscous shock layer theory and the preferential vibration-dissociation-exchange reactions coupling model, which takes into account the interaction between the vibrational relaxation and the chemical processes, are used as an initial gasdynamics model. The efficient computational algorithm on based high-accuracy implicit finite difference scheme is used. The algorithm does not imply the existence of a symmetry plane in the flow and does not need a preliminary solution to the Stefan–Maxwell relations with respect to the diffusion fluxes. The influence of the body shape, of the attack and slip angles, of the heterogeneous chemical reaction model, of the freestream parameters, and of the vibrational nonequilibrium on the heat flux and on the equilibrium surface temperature is investigated.

I. Introduction: Problem Statement

VIBRATIONAL relaxation and chemical processes are significant during the hypersonic reentry phase of a space vehicle because the total enthalpy of the freestream flow is large enough to cause vibrational excitation and molecular dissociation in the shock layer. The air gas is then assumed to be composed of five species, N, O, NO, N_2, and O_2, governed by a 17-chemical-reaction scheme: 15 dissociation–recombination reactions and 2 exchange reactions; ionization is neglected. The molecules N_2 and O_2 are considered in vibrational nonequilibrium, whereas NO is assumed to be in vibrational equilibrium because of its small vibrational relaxation timescale in comparison with the characteristic flow timescale. On the other hand, the order of magnitude of the relaxation timescales of the vibrational processes and of the chemical reactions are similar, which leads to a strong coupling between these nonequilibrium phenomena. This coupling includes, on one hand, the influence of the vibrational relaxation on the chemical reactions and on the other hand the reverse effect. Hammerling et al.[1] considered the influence of the vibrational excitation of the molecules on their dissociation and proposed a model called coupled vibration–dissociation (CVD). This aspect of the coupling leads to an increase or decrease in the forward kinetic rate constant. Then Marrone and Treanor[2] completed this model by also considering the influence of the molecule dissociation on the average vibrational energy of the molecules [coupled vibration–dissociation–vibration (CVDV)], the vibrational relaxation of N_2 and O_2 being modified through vibration–chemistry exchanges in addition to the usual vibration–translation energy exchanges. Park[3] proposed a two-temperature model to describe the CVD, built on an empirical formula fitting experimental data. All of these models have been derived for dissociation reactions only and do not take into account the exchange reactions. However, recently, several authors have developed new models for the full vibration–chemistry coupling.[4–7] In this connection, Séror et al.[8,9] proposed the coupled vibration–dissociation–exchange reactions (CVDEV) model with a preferential formulation of the coupling factor for exchange reactions. It is this CVDEV model that is used in the present work.

Just behind the shock wave, the translational temperature reaches its peak value while the vibrational temperature lags because it takes a finite time for the vibration to be excited. The estimations also show that the gradients of the vibrational temperatures and the fluxes of the vibrational energy in the relaxation zone just behind the shock wave are rather large; therefore, for an accurate description of this sublayer, it is necessary to take into account the molecular transfer effects in this zone. In this connection as an initial gasdynamics model we use the thin viscous shock layer (TVSL) theory, which was initially suggested for two-dimensional hypersonic viscous gas flow by Cheng[10] and then extended to three-dimensional nonequilibrium multicomponent hypersonic viscous flows by Gershbein.[11] From a mathematical point of view, the TVSL equations system is a composite one because it contains all of the terms of boundary-layer equations and all of the terms of the hypersonic approximation of inviscid shock layer equations.[12] The attractiveness of this model for practical applications is explained by at least two reasons. First, as demonstrated with comparisons of solutions obtained with more complete mathematical flow models and experimental data, the TVSL model gives a high accuracy of the flow parameters on the stagnation region of the body surface, where the shock layer is sufficiently thin and the heat fluxes are maximum.[13] The second reason is that the TVSL equation system is of parabolic type, which permits us to apply a fast and economical marching numerical procedure for obtaining the solution and, by this means, to increase greatly the computation efficiency. Today the TVSL model is widely applied for three-dimensional hypersonic viscous gas flow calculations[14,15] because it has a correct asymptotical character, it adequately describes the flowfield between a shock wave and the body surface, and it takes into account the molecular transfer effects near the body surface as well as near the shock wave.

The aim of this paper is to apply the thermochemical nonequilibrium model (CVDEV model) and the TVSL approach for three-dimensional hypersonic airflow computations around a blunt body moving along a prescribed aerodynamic reentry trajectory.

Received 1 May 1999; presented as Paper 99-3628 at the AIAA 33rd Thermophysics Conference, Norfolk, VA, 28 June–1 July 1999; revision received 5 May 2000; accepted for publication 19 September 2000.

*Professor, Head of Computational Fluid Dynamics Laboratory, Institute of Applied Mathematics and Mechanics, Lenina 36.

†Research Scientist, Institute of Applied Mathematics and Mechanics, Lenina 36.

‡Centre National de la Recherche Scientifique Research Scientist, Institut Universitaire des Systèmes Thermiques Industriels, Technopôle de Château-Gombert. Member AIAA.

§Research Scientist, Institut Universitaire des Systèmes Thermiques Industriels, Technopôle de Château-Gombert.

¶Professor, Institut Universitaire des Systèmes Thermiques Industriels, Technopôle de Château-Gombert. Senior Member AIAA.

The joint influence of the vibration–chemistry nonequilibrium coupling and of the molecular transfer effects on the body surface heat flux, as well as on the structure of the shock layer, is investigated. Numerous computations highlight interesting results. It is shown that, at the stagnation line, the ratio of wall equilibrium temperature $T_w(k)/T_w(1)$ (where k is the ratio of the main curvatures of the reentry bodies and is equal to 1 for a sphere) is quite conservative for different trajectory points and different wall catalysis models. The isovalues of $T_w(1)$ on a sphere for a wide range of flight altitude and freestream velocity along the reentry trajectory will be also given for a pratical use. It is also shown that the distributions of the wall heat flux referred to their values at the stagnation point have a conservative behavior and depend very little on the trajectory point, on the catalysis models, or on the linear size of the body, but do depend on the body shape and on the values of the attack and slip angles. This result is used to suggest an approximate approach that gives results close to the complete numerical ones.

II. Governing Equations

The TVSL equation system written in a curvilinear coordinate system x^k and describing the three-dimensional viscous thermochemical nonequilibrium multicomponent gas flow between the shock and the body surface including nonequilibrium chemical reactions, vibrational relaxation, vibration–chemistry coupling, and multicomponent diffusion and excluding barodiffusion, thermodiffusion, and diffusion thermoeffect have the following dimensionless form.[13]

Continuity equation:

$$D_k\left(\rho u^k a^{\frac{1}{2}} a_{(kk)}^{-\frac{1}{2}}\right) = 0 \tag{1}$$

Momentum equations:

$$\rho A^3_{\beta\delta} u^\beta u^\delta = -D_3 P, \qquad D_3 P_\alpha = -D_\alpha\left(\rho A^3_{\delta\beta} u^\delta u^\beta\right) \tag{2}$$

$$\rho\left(Du^\alpha + A^\alpha_{\beta\delta} u^\beta u^\delta\right) = -a^{\alpha\beta} a_{(\alpha\alpha)}^{\frac{1}{2}} P_\beta + D_3\left[(\mu/Re) D_3 u^\alpha\right] \tag{3}$$

Energy equation:

$$\begin{aligned}\rho\left(c_p DT - \sum_{i=1}^{N_M} c_i De^*_{v_i}\right) &= 2u^\alpha a_{(\alpha\alpha)}^{-\frac{1}{2}} P_\alpha \\ &+ D_3\left(\frac{\mu c_p}{\sigma Re} D_3 T - \sum_{i=1}^{N_M} c_i \frac{\mu}{ReSc_{v_i}} D_3 e^*_{v_i}\right) \\ &+ \frac{2\mu}{Re} B_{\alpha\beta} D_3 u^\alpha D_3 u^\beta - D_3 T \sum_{j=1}^{N} c_{pj} I_j \\ &+ \sum_{i=1}^{N_M} I_i D_3 e^*_{v_i} - \sum_{j=1}^{N} h^0_j \dot\omega_j + \sum_{i=1}^{N_M} e^*_{v_i} \dot\omega_i\end{aligned} \tag{4}$$

Species conservation equations:

$$\rho Dc_j + D_3 I_j = \dot\omega_j, \qquad j = 1, \ldots, N-1 \tag{5}$$

Vibrational energy conservation equations:

$$\rho c_i De_{v_i} + I_i D_3 e_{v_i} = \rho c_i \dot\Omega_i + D_3\left[c_i\left(\mu/ReSc_{v_i}\right) D_3 e_{v_i}\right] \qquad i = 1, \ldots, N_M \tag{6}$$

Equation of state:

$$P = \rho T \frac{R_A T_0}{V_\infty^2} \sum_{j=1}^{N} \frac{c_j}{m_j} \tag{7}$$

where

$$D_k = \frac{\partial}{(\partial x^k)}, \qquad D^* = u^\alpha a_{(\alpha\alpha)}^{-\frac{1}{2}} D_\alpha, \qquad D = D^* + u^3 D_3$$

$$P_\alpha \equiv \frac{\partial P}{\partial x^\alpha}, \qquad \sum_{j=1}^{N} c_j = 1, \qquad \sum_{j=1}^{N} I_j = 0$$

$$c_p = \sum_{j=1}^{N} c_{pj} c_j, \qquad B_{\alpha\beta} = a_{\alpha\beta} a_{(\alpha\alpha)}^{-\frac{1}{2}} a_{(\beta\beta)}^{-\frac{1}{2}}$$

$$e^*_{v_i} = e^{N_i}_{v_i}(T) - e^{N_i}_{v_i}\left(T_{v_i}\right), \qquad Re = \frac{\rho_\infty V_\infty L}{\mu(T_0)}, \qquad \sigma = \frac{\mu c_p}{\lambda}$$

$$Sc_{v_i} = \frac{\mu}{\rho D_{v_i}}, \qquad D_{v_i} = \left[\sum_{j=1}^{N} \frac{mc_j}{m_j D_{ij}}\right]^{-1}, \qquad T_0 = 10^4\ \mathrm{K}$$

$$e^{N_i}_{v_i} = \frac{R_A \theta_{v_i}}{m_i\left[\exp\left(\theta_{v_i}/T_{v_i}\right) - 1\right]} - \frac{N_i R_A \theta_{v_i}}{m_i\left[\exp\left(N_i\theta_{v_i}/T_{v_i}\right) - 1\right]}$$

The closing relations to this system are the Stefan–Maxwell equations:

$$\frac{\mu}{Re} \sum_{k=1}^{N} \frac{1}{m_i m_k}(c_k D_3 c_i - c_i D_3 c_k) = \sum_{k=1}^{N} \frac{Sc_{ik}}{m_i m_k}(c_i I_k - c_k I_i) \tag{8}$$

If we take into account the conditions

$$\sum_{k=1}^{N} c_k = 1, \qquad \sum_{k=1}^{N} I_k = 0$$

and exclude c_N and I_N from Eq. (8), these relations can be rewritten in the following form, which is more convenient for numerical calculations:

$$I_j = \alpha_j D_3 c_j + \beta_j c_j, \qquad \alpha_j = -\frac{\mu b_{(jj)}}{ReSc_{lN} a_{(jj)}}$$

$$\beta_j = a_{jj}^{-1} \sum_{k=1, k\neq j}^{N} \left(a_{jk} I_k + \frac{\mu b^*_k}{ReSc_{lN}} D_3 c_k\right)$$

$$a_{jk} = -a^*_{jk} c_j, \qquad b_{jk} = b^*_k c_j, \qquad (k \neq j)$$

$$a^*_{jk} = \frac{m_j}{m_k}\frac{Sc_{jk}}{Sc_{lN}} - \frac{Sc_{jN}}{Sc_{lN}}, \qquad b^*_k = \frac{m_N}{m_k} - 1$$

$$a_{jj} = \frac{Sc_{jN}}{Sc_{lN}} + \sum_{k=1, k\neq j}^{N} a^*_{jk} c_k, \qquad b_{jj} = 1 + \sum_{k=1, k\neq j}^{N} b^*_k c_k \tag{9}$$

System (1–9) is solved with boundary conditions on the shock wave and on the body surface. On the shock wave, the hypersonic approximation of the generalized Rankin–Hugoniot conditions are used to take into account the effects of molecular transfer into the shock wave:

$$\begin{aligned}&x^3 = x^3_s(x^1, x^2): \qquad \rho\left(u^3 - D^* x^3_s\right) = u^3_\infty, \qquad P = \left(u^3_\infty\right)^2 \\ &P_\alpha = 2u^3_\infty D_\alpha\left(u^3_\infty\right), \qquad u^3_\infty\left(u^\alpha - u^\alpha_\infty\right) = \frac{\mu}{Re} D_3 u^\alpha \\ &\frac{\mu c_p}{\sigma Re} D_3 T - \sum_{i=1}^{N_M} c_i \frac{\mu}{ReSc_{v_i}} D_3 e^*_{v_i} = u^3_\infty\left[\sum_{j=1}^{N} c_{j\infty}\left(h^0_j - h^0_{j\infty}\right)\right. \\ &\qquad \left. - \sum_{i=1}^{N_M} c_{i\infty} e^*_{v_i} - \left(u^3_\infty\right)^2 - B_{\alpha\beta}\left(u^\alpha - u^\alpha_\infty\right)\left(u^\beta - u^\beta_\infty\right)\right] \\ &u^3_\infty(c_j - c_{j\infty}) + I_j = 0, \qquad j = 1, \ldots, N-1 \\ &\frac{\mu}{ReSc_{v_i}} c_i D_3 e^*_{v_i} = u^3_\infty c_{i\infty}\left(e^*_{v_i} - e^*_{v_i\infty}\right), \qquad i = 1, \ldots, N_M\end{aligned} \tag{10}$$

On the body surface, heterogeneous chemical reactions are taken into account, but heat discharge inward of the body is neglected:

$$x^3 = 0: \qquad u^k = 0, \qquad I_j = \dot{r}_j$$

$$k = 1, 2, 3, \qquad j = 1, \ldots, N-1$$

$$\frac{\mu c_p}{\sigma Re} D_3 T - \sum_{j=1}^{N} I_j h_j^0 - \sum_{i=1}^{N_M} \left(\frac{\mu c_i}{ReSc_{v_i}} D_3 e_{v_i}^* - I_i e_i^* \right) = GT^4$$

$$G = 2\varepsilon_B \sigma_B T_0^4 \Big/ \left(\rho_\infty V_\infty^3\right) \quad (11)$$

Here x^3 is directed along the outward normal to the body surface, and x^1 and x^2 are selected on the surface, with the origin at the stagnation point $x^1 = 0$. We assume the summation for repeating subscripts not enclosed in brackets. Latin indices are equal to 1, 2, or 3, excluding the special marked cases. Greek indices are equal to 1 or 2. $V_\infty u^k$ are the physical components of the vector velocity; $V_\infty^2 \rho_\infty P$, $\rho_\infty \rho$, and $T_0 T$, are, respectively, the dimensional pressure, the density, and the temperature of the gas mixture that consists of N components (including N_M molecules). Here $\mu_0 \mu$, $V_\infty^2 c_p/(2T_0)$, σ, and m are, respectively, the viscosity, the specific heat at constant pressure, the Prandtl number, and the molecular mass of the mixture, whereas c_j, m_j, $V_\infty^2 h_j/2$, $V_\infty^2 e_{v_i}/2$, $T_0 T_{v_i}$, $T_0 \theta_{v_i}$, N_i, $V_\infty^2 c_{pj}/(2T_0)$, $V_\infty \rho_\infty I_j$, $V_\infty \rho_\infty \dot{\omega}_j / L$, $V_\infty^3 \dot{\Omega}_i / 2L$, and Sc_{ij} are the mass concentration, the molecular mass, the specific enthalpy, the vibrational energy, the vibrational temperature, the specific vibrational temperature, the number of vibrational levels of the molecule, the specific heat, the normal component of a diffusion flux vector, the formation rate of the jth species, the formation rate of the vibrational energy of the ith molecule, and the binary Schmidt number. L is the characteristic linear size of the problem, $a_{\alpha\beta}$ and $b_{\alpha\beta}$ are the covariant components of the first and second quadratic form of the body surface, ε_B is a coefficient of the surface blackness, σ_B is the Stefan–Bolzmann constant, and $A_{\alpha\beta}^k$ are the known functions of the body shape.[13] The subscripts w, ∞, and s correspond, respectively, to values on the body surface, at infinity, and behind the shock wave; the subscript 0 corresponds to the case where the vibrational mode is considered in equilibrium with the translational energy.

It is assumed that the catalytic reactions on the body surface are the following first-order reactions:

$$\dot{r}_j = -\rho k_{wj} c_j, \qquad j = \mathrm{O}, \mathrm{N}, \mathrm{NO}$$

where k_{wj} are the kinetic rate constants of the heterogeneous reactions. Three models of heterogeneous chemical reactions are considered.

Noncatalytic surface:

$$k_w(\mathrm{O}) = k_w(\mathrm{N}) = 0 \quad (12)$$

Ideal catalytic surface:

$$k_w(\mathrm{O}) = k_w(\mathrm{N}) = \infty \quad (13)$$

Finite catalytic surface:

$$V_\infty k_w(\mathrm{O}) = 10.4 \text{ m/s}, \qquad V_\infty k_w(\mathrm{N}) = 3 \text{ m/s} \quad (14)$$

Model (14) corresponds to the experimental data.[16] It is assumed everywhere that $k_w(\mathrm{NO}) = 0$.

III. Thermochemical Model

Air is simulated by the five-component mixture, N, O, NO, N_2, and O_2, where dissociation–recombination reactions $O_2 + M = 2O + M$, $N_2 + M = 2N + M$, $NO + M = N + O + M$, and exchange reactions $N + O_2 = NO + O$, $O + N_2 = NO + N$ take place; M is the third particle in the reaction, to be chosen among the species N_2, O_2, NO, N, and O. The temperature dependencies of direct and reverse reaction constants are defined from Ref. 17 using the temperature T. To compute the mixture transport coefficients and thermodynamic quantities data from Refs. 18–20 are used.

Taking into account the coupling of the vibration on the chemical processes amounts to modifying the forward dissociation reaction rates k_f as follows[1,2,5]:

$$k_{fi}^* = V_{D_i} k_{fi} \quad (15)$$

where V_{D_i} is the coupling factor written with the partition functions Q as follows:

$$V_{D_i} = \frac{Q^{N_{D_i}}(T)\, Q^{N_{D_i}}\left(T_{f_i}\right)}{Q^{N_{D_i}}\left(T_{v_i}\right) Q^{N_{D_i}}\left(-U_{D_i}\right)}$$

$$Q^{N_{D_i}}(X) = \frac{1 - \exp\left(-N_{D_i}\theta_{v_i}/X\right)}{1 - \exp\left(-\theta_{v_i}/X\right)} \quad (16)$$

where T_{v_i} is the vibrational temperature of the species i and T_{f_i} is an average temperature written as

$$1/T_{f_i} = 1/T_{v_i} - 1/T - 1/U_{D_i}$$

where $(-U_{D_i})$, having the dimension of a temperature, expresses the probability of dissociation starting from a certain vibrational energy level. Thus, for $U_{D_i} = \infty$, the dissociation is equiprobable from any vibrational energy level (nonpreferential coupling), whereas with a lower value of U_{D_i}, the probability of dissociation is increased for higher vibrational energy levels (preferential regime). The value of U_{D_i} is thought to be of the order of magnitude of the dissociation characteristic temperature θ_{D_i} (Ref. 2). The values of θ_{v_i} (Kelvin), θ_{D_i} (Kelvin), U_{D_i}, and $N_{D_i} = E(\theta_{D_i}/\theta_{v_i}) + 1$, that is, the number of vibrational levels of the molecule i considered as a harmonic oscillator truncated just above the dissociation energy θ_{D_i}, are as follows:

$$\theta_{v_{O_2}} = 2240, \qquad \theta_{D_{O_2}} = 59{,}500, \qquad N_{D_{O_2}} = 27$$

$$U_{D_{O_2}} = \theta_{D_{O_2}}/2, \qquad \theta_{v_{N_2}} = 3354, \qquad \theta_{D_{N_2}} = 113{,}200$$

$$N_{D_{N_2}} = 34, \qquad U_{D_{N_2}} = \theta_{D_{N_2}}/6$$

For exchange reactions, a coupling factor V_{E_i} is used in place of V_{D_i} in Eq. (15) with the following expression[8]:

$$V_{E_i} = \frac{Q^{N_{D_i}}(T)}{Q^{N_{D_i}}\left(T_{v_i}\right)} \frac{S_i}{R_i}, \qquad \frac{1}{T_{F_i}} = \frac{1}{T_{v_i}} - \frac{1}{T} - \frac{1}{U_{E_i}}$$

$$S_i = Q^{N_{A_i}}\left(T_{F_i}\right) \exp\left(-\frac{\epsilon_{A_i}}{U_{E_i}}\right) + Q^{N_{D_i} - N_{A_i}}\left(T_{v_i}\right) \exp\left(\frac{\epsilon_{A_i}}{T} - \frac{\epsilon_{A_i}}{\alpha_i T_{v_i}}\right)$$

$$R_i = Q^{N_{A_i}}\left(-U_{E_i}\right) \exp\left(-\frac{\epsilon_{A_i}}{U_{E_i}}\right) + Q^{N_{D_i} - N_{A_i}}(T) \exp\left(\frac{\alpha_i - 1}{\alpha_i} \frac{\epsilon_{A_i}}{T}\right) \quad (17)$$

The values of ϵ_{A_i} (Kelvin), U_{E_i}, α_i, and N_{A_i}, that is, the number of vibrational levels of the molecule i considered as a harmonic oscillator truncated just above the activation energy ε_{A_i}, are as follows:

$$\epsilon_{A_{O_2}} = 3{,}020, \qquad N_{A_{O_2}} = 2, \qquad U_{E_{O_2}} = \frac{\epsilon_{A_{O_2}}}{5}, \qquad \alpha_i = \frac{\epsilon_{A_i}}{N_{A_i}\theta_{v_i}}$$

$$\epsilon_{A_{N_2}} = 37{,}750, \qquad N_{A_{N_2}} = 12, \qquad U_{E_{N_2}} = \frac{\epsilon_{A_{N_2}}}{5}$$

Note that the coupling model modifies the forward rate constant but not the backward constant; indeed, it is implicitly supposed that the recombination of molecules does not depend on the vibrational excitation.

To each of the two molecules in vibrational nonequilibrium, an equation is attached, governing the evolution of its vibrational energy, that is, of its vibrational temperature under the harmonic oscillator assumption. The source terms $\dot{\Omega}_i$ of Eqs. (6) are made up of two terms that mirror the various exchanges between the modes: translation–vibration $\dot{\Omega}_i^{\mathrm{T-V}}$ and chemistry–vibration coupling $\dot{\Omega}_i^{\mathrm{C-V}}$.

The energy exchanges between vibrational and translational modes are classically described by the Landau–Teller formula[21]

$$\dot{\Omega}_i^{\mathrm{T-V}} = \frac{e_{v_i}^{N_{D_i}}(T) - e_{v_i}^{N_{D_i}}(T_{v_i})}{\tau_i^{\mathrm{VT}}}, \qquad \frac{1}{\tau_i^{\mathrm{VT}}} = \sum_{j=1}^{N} \frac{mc_j}{m_j \tau_{ij}^{\mathrm{VT}}} \tag{18}$$

where τ_i^{VT} is the global relaxation time and τ_{ij}^{VT} is the relaxation time for the vibrational–translational exchange between a molecular species i and any species j (Refs. 22–24).

The chemical–vibrational coupling proceeds from the fact that the vibrational energy of a molecule is partially determined by the chemical relaxation process. Following Refs. 2 and 8, one can write

$$\dot{\Omega}_i^{\mathrm{C-V}} = \dot{\Omega}_i^{D} + \dot{\Omega}_i^{E}$$

where $\dot{\Omega}_i^{D}$ and $\dot{\Omega}_i^{E}$ are as follows:

$$\dot{\Omega}_i^{D} = \left(\dot{\omega}_i^{g,D}/\rho_i\right)\left[e_{v_i}^{N_{D_i}}(-U_{D_i}) - e_{v_i}^{N_{D_i}}(T_{v_i})\right] - \left(\dot{\omega}_i^{l,D}/\rho_i\right)\left[e_{v_i}^{N_{D_i}}(T_{f_i}) - e_{v_i}^{N_{D_i}}(T_{v_i})\right] \tag{19}$$

$$\dot{\Omega}_i^{E} = \left(\dot{\omega}_i^{g,E}/\rho_i\right)\left[e_{v_i}^{g,E} - e_{v_i}^{N_{D_i}}(T_{v_i})\right] - \left(\dot{\omega}_i^{l,E}/\rho_i\right)\left[e_{v_i}^{l,E} - e_{v_i}^{N_{D_i}}(T_{v_i})\right] \tag{20}$$

where $\dot{\omega}_i^{g,D}$ and $\dot{\omega}_i^{l,D}$ are the rates of creation and destruction of the molecule $i = \mathrm{O}_2$ and N_2 in the first two dissociation reactions. The values $e_{v_i}^{l,E}$ and $e_{v_i}^{g,E}$ are the vibrational energy loss and gain through an exchange reaction and read

$$e_{v_i}^{l,E} = \frac{A_1^{l_i} + A_2^{l_i}}{A_3^{l_i} + A_4^{l_i}}, \qquad e_{v_i}^{g,E} = \lim_{T_{v_i} \to T} e_{v_i}^{l,E}$$

$$A_1^{l_i} = \exp\left(-\frac{\epsilon_{A_i}}{U_{E_i}}\right) Q^{N_{A_i}}(T_{F_i}) e_{v_i}^{N_{A_i}}(T_{F_i})$$

$$A_2^{l_i} = \exp\left(\frac{\epsilon_{A_i}}{T}\right)\left[Q^{N_{D_i}}(T_{v_i}) e_{v_i}^{N_{D_i}}(T_{v_i}) - Q^{N_{A_i}}(T_{v_i}) e_{v_i}^{N_{A_i}}(T_{v_i})\right]$$

$$A_3^{l_i} = \exp\left(-\frac{\epsilon_{A_i}}{U_{E_i}}\right) Q^{N_{A_i}}(T_{F_i})$$

$$A_4^{l_i} = \exp\left(\frac{\epsilon_{A_i}}{T} - \frac{\epsilon_{A_i}}{\alpha_i T_{v_i}}\right) Q^{N_{D_i} - N_{A_i}}(T_{v_i}) \tag{21}$$

IV. Numerical Method

For the numerical solution to the problem, the cylindrical coordinate system (x^1, x^2) related to the body surface is chosen, with the origin at the stagnation point $x^1 = 0$ (with x^1 the marching coordinate and x^2 the circumferential coordinate; see Fig. 1).[14] This coordinate system enables us to obtain the undegenerable equations for longitudinal and circumferential gradients of pressure P_α and to solve the closing problem of the equations system at the lateral body surface.

So far, because this coordinate system degenerates at the stagnation point, the undegenerated curvilinear coordinate system $\{t^k\}$ is used to solve the initial equations at the stagnation point. The axes Ot^1 and Ot^2 are directed along the main directions of the body surface at the stagnation point, and the axis Ot^3 coincides with the normal to the body surface. After that the solution to the initial equations at the stagnation point in the $\{t^k\}$ coordinate system is recalculated for the $\{x^k\}$ coordinate system and then used as the initial condition for system (2–7) on the line $x^1 = 0$.

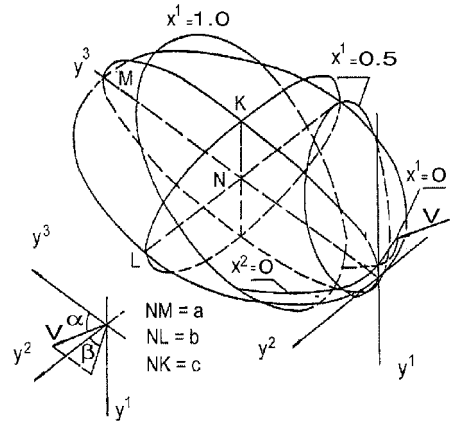

Fig. 1 Schematic of the coordinate system used at the body surface, with attack and slipping angles α and β.

The initial equation system is written in variables of Dorodnicyn type, and in this way the singularities of the initial equations at the stagnation line are resolved:

$$\xi^\alpha = x^\alpha, \qquad \zeta = \Delta^{-1}\int_0^{x^3} \rho\, \mathrm{d}x^3, \qquad \Delta = \int_0^{x_s^3} \rho\, \mathrm{d}x^3$$

$$\Theta = \frac{T}{T_*}, \qquad l = \frac{\mu\rho}{Re\Delta^2}, \qquad u^\alpha = D_3 f_\alpha$$

$$P_\alpha = (\xi^\alpha)^{-1} D_\alpha P, \qquad X_j = \frac{I_j}{\Delta}, \qquad u_*^\alpha = u_\infty^\alpha$$

$$T_* = \left(u_\infty^3\right)^2, \qquad \rho u^3 a^{\frac{1}{2}} = -D_\alpha\left(\psi_{(\alpha)}^* f_\alpha\right) - \psi_{(\alpha)}^* D_3 f_\alpha \frac{\partial\zeta}{\partial x^\alpha}$$

$$\psi_{(\alpha)}^* = \Delta a^{\frac{1}{2}} \phi_\alpha^* = \frac{\Delta a^{\frac{1}{2}} u_*^\alpha}{a_{(\alpha\alpha)}^{\frac{1}{2}}} \tag{22}$$

The numerical solution to the problem is obtained on the basis of an implicit finite difference method relative to ζ (Ref. 15), which is $\mathcal{O}(\Delta\xi^1) + \mathcal{O}(\Delta\xi^2)^2 + \mathcal{O}(\Delta\zeta)^4$ accuracy order and the generalization of well-known high-order approximation schemes.[25] In general, the use of high-order approximation schemes leads to two consequences: First, the value of the computer memory is increased. Second, the algorithm of the solution is more complicated than widely practiced two-order approximation schemes. However, high-order accurate schemes for smooth flows can considerably decrease the total number of grid points and, therefore, gain advantage over second-order schemes, both on the computer memory and on the CPU time. This is more obvious for three-dimensional viscous reacting gas flows, where the application of high-order approximation schemes is often the only way to obtain the solution to the problem in an acceptable calculation time. For the convective operator, the approximations of derivatives with respect to the marching coordinate ξ^1 are replaced by backward difference operators, and the derivatives with respect to the circumferential coordinate ξ^2 are replaced by central difference operators on the basis of the solution obtained during the previous global iteration on the current circle $\xi^1 + \Delta\xi^1 = \mathrm{const}$. As a result of the nonlinear character of the equation system in each circle $\xi^1 + \Delta\xi^1 = \mathrm{const}$, the global iteration process is organized, and the thickness of the shock layer is calculated by means of a cyclical three-diagonal solver method on the coordinate ξ^2. To increase the computational accuracy at high Reynolds numbers, the numerical mesh is compressed near the body surface and near the shock layer.

The important property of this numerical procedure is that it does not need a preliminary solution to the Stefan–Maxwell equations with respect to the diffusion fluxes and it does not imply flow symmetry planes, which enables us to investigate the three-dimensional flow around bodies at the attack and slip angles.

V. Results and Discussion

On the basis of the TVSL model and of the numerical algorithm presented earlier, the hypersonic nonequilibrium multicomponent airflow at angle of attack α and slipping angle β over the catalytic surface of ellipsoid with axis ratio $a{:}b{:}c$ is investigated (see Fig. 1). The computations are done by considering the vibrational and chemical nonequilibrium processes and the coupling between them. The upstream conditions correspond to different points of a space shuttle trajectory.[26] The governing parameters of the problem, altitude H, velocity V_∞, and linear size L of the reentry body, vary in the following range: $50 \le H \le 100$ km, $2.0 \le V_\infty \le 8.0$ km/s, and $0.05 \le L \le 5.0$ m, and the blackness coefficient is $\varepsilon_B = 0.85$. To verify the present method, the numerical results have been compared to numerical solutions to Euler equations coupled to the asymptotic defect boundary-layer approach[27,28] for Lobb experiment conditions,[29] to numerical solutions to the parabolized Navier–Stokes equations (results from Brueck[30] for hyperboloid geometry and results from Fujiwara and Aso[31] for OREX configuration), and to experimental data from Ref. 32. These comparisons of the heat flux absolute value q_w (MW/m^2) at the stagnation point of the body surface are presented in Table 1: The agreement between the results is satisfactory. Comparisons of the equilibrium temperature T_w along the sphere surface ($H = 35$, 5 km, $V_\infty = 5.26$ km/s, and $L = 6.35$ mm) between the present computations and the numerical solution to the Euler equations coupled to the asymptotic defect boundary-layer equations[27] are presented in Fig. 2a: The agreement between the two solutions is satisfactory. Note that the solution in Refs. 8, 9, and 27 has already been validated by comparisons with other results and experimental data. Comparisons of the heat flux absolute value q_w along a symmetry plane of the ellipsoid surface (with axis 1:0.25:0.417 for $H = 26.6$ km, $V_\infty = 3.62$ km/s, and $L = 0.18$ m) with the experimental data[32] are presented in Fig. 2b.

The influence of the mesh point number M_3 across the shock layer on the computation accuracy of the body surface equilibrium temperature T_w is smaller than 1% as soon as $M_3 \ge 10$. These computational data correspond to the stagnation point of a flow around an ellipsoid 1:0.7:0.3, whose surface is ideal catalytic and with $\alpha = \beta = 0$ deg, $L = 0.5$ m, $V_\infty = 7.25$ km/s, and $H = 70$ km. On the lateral body surface, the influence of M_3 is similar to its influence on the stagnation point. As for the influence of the number of grid points M_1 and M_2 along the surface coordinates x^1 and x^2 on the absolute value of the wall equilibrium temperature T_w, one

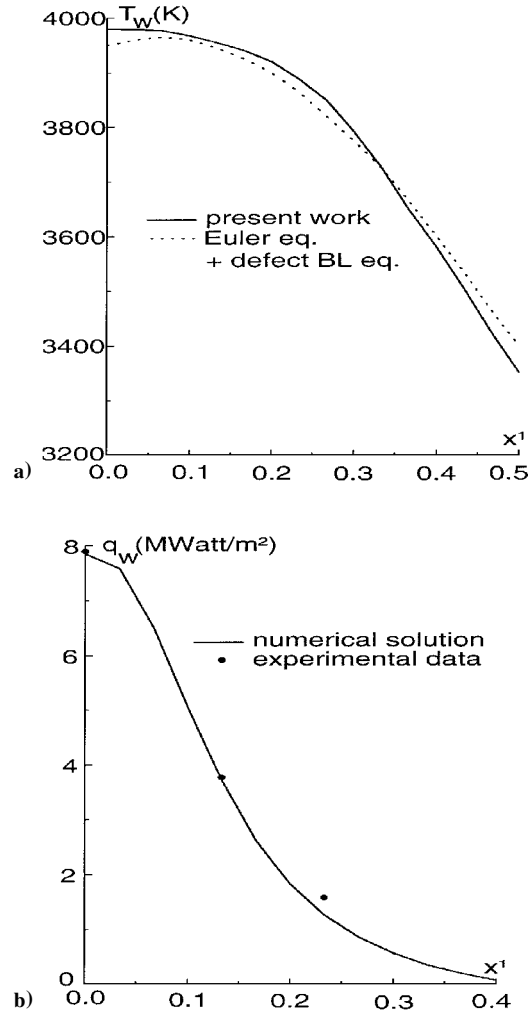

Fig. 2 Equilibrium wall temperature $T_w(K)$ and the heat flux q_w (MW/m^2) distributions along the ellipsoid surface; comparisons of the present results with other numerical results and with experimental data.

Table 1 Comparisons between the present results and reference results: absolute value of heat flux q_w (MW/m^2) at stagnation point for different freestream conditions and catalysis models

V_∞, km/s	H, km	Catalysis model	Ref.	Ref. value	Present work
5.26	35.5	(12)	27	22.72	23.01
5.26	35.5	(13)	27	33.73	34.01
7.45	91.0	(12)	30	0.096	0.098
5.56	58.0	(12)	30	0.345	0.350
5.56	58.0	(13)	30	0.516	0.513
3.90	63.0	(12)	31	0.148	0.151
3.62	26.6	(13)	32	7.884	7.845
3.57	46.8	(13)	32	1.623	1.626

Table 2 Values of the wall equilibrium temperature $T_w(K)$ for different grids

x^2	$H_{30\times32}$	$H_{30\times48}$	$H_{30\times64}$	$H_{30\times128}$	$H_{15\times64}$	$H_{50\times64}$
0.26	2247	2276	2289	2292	2310	2290
1.31	2121	2147	2158	2160	2180	2157
2.36	2015	2036	2040	2042	2062	2038
3.01	2091	2109	2115	2116	2136	2111
4.06	1847	1832	1828	1827	1846	1823
4.97	1390	1366	1351	1349	1368	1345
5.76	1890	1875	1870	1869	1887	1866

example of this dependency is given in Table 2, where the values T_w at $x^1 = 0.3$ and at different values x^2 for different grids $H_{M_1\times M_2}$ are presented. These tests are done for the following conditions: $H = 70$ km, $L = 0.5$ m, $V_\infty = 7.25$ km/s, $\alpha = \beta = 45$ deg, $M_3 = 10$, and noncatalytic wall.

On the whole, the systematic numerical simulation enables us to draw the conclusion that, for a solution with an error lower than 1.0%, a mesh with $M_1 = 30$, $M_2 = 64$, and $M_3 = 10$ can be used (M_α is the number of grid points along the coordinate x^α) with coordinate x^1 and 64 points on circumferential. Analysis of the numerical calculations also shows that the suggested algorithm is stable, has a high level of arithmetical cost efficiency, the CPU time for one variant of computation on a Hewlett–Packard 712/80 is about 15–20 min, and enables variants for a wide range of flight altitude and freestream velocity to be computed rapidly.

A. Three-Dimensional Stagnation Line

First, we present the numerical results along a three-dimensional stagnation line. The problem solution at this location depends on one geometrical parameter only because of the parabolic type of the equations. It is the value $k = R_1/R_2$, where R_1 and R_2 are the main curvatures of the body surface at the stagnation point. Case $k = 1.0$, one limit case, corresponds to the stagnation point of a sphere; case $k = 0.0$, the other limit case, corresponds to the stagnation point of a cylinder; and the case $0 < k < 1.0$ corresponds to an intermediate geometry.

In Fig. 3, the distributions of the equilibrium wall temperature T_w on the body surface at the stagnation point as a function of the altitude H along the space shuttle trajectory are shown[26]: Fig. 3a

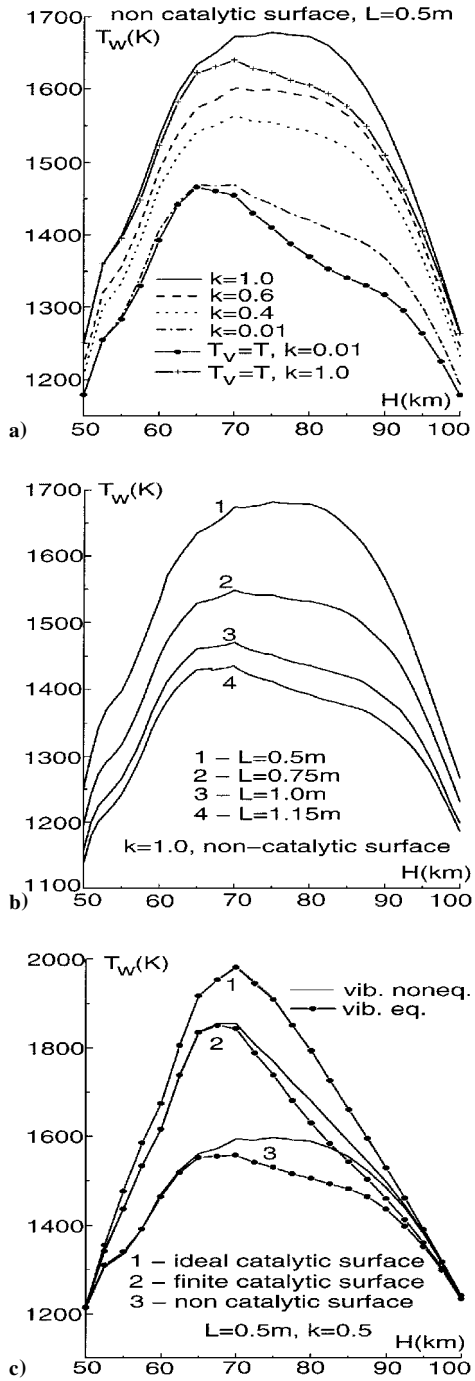

Fig. 3 Equilibrium wall temperature T_w at three-dimensional stagnation point vs the flight altitude H(km) for different k, L, and for different catalysis models.

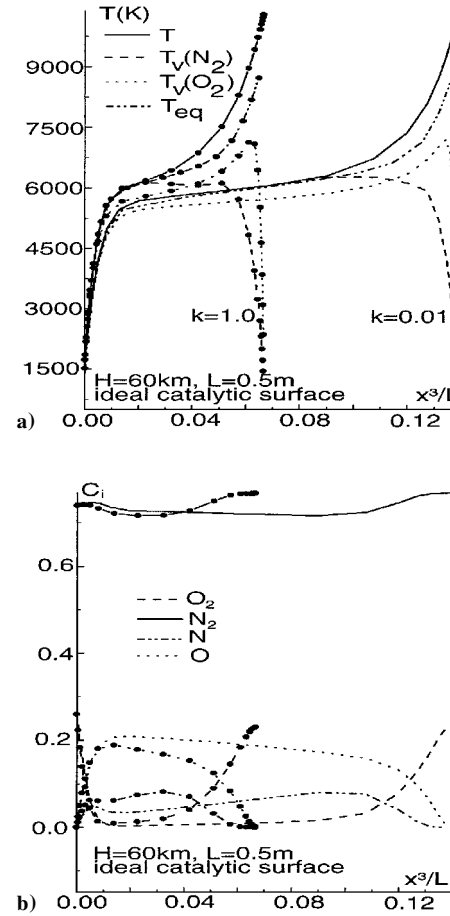

Fig. 4 $L = 0.5$ m, and $k = 1.0$ (lines with circles) and $k = 0.01$ (lines without circles): a) profiles of the transrotational and vibrational temperatures and b) profiles of the mass fractions of the components across the shock layer at the stagnation line.

for a noncatalytic surface, for a given linear size $L = 0.5$ m and for different values of the parameter k; Fig. 3b for a noncatalytic surface, for a given parameter $k = 1.0$ and for different sizes L; and Fig. 3c for a given size $L = 0.5$ m, a given parameter $k = 0.5$, and for different wall heterogeneous chemical reaction models. These results correspond to computations with vibrational nonequilibrium, but results obtained with vibrational equilibrium are also plotted. The solutions show that for a considered trajectory the absolute value of the heat flux q_w (or the wall equilibrium temperature T_w) on the body surface is a nonmonotonic function of the flight altitude and presents a maximum. The position of this maximum depends on the geometrical parameters k and L, as well as on the vibrational relaxation effects and on the wall catalysis heterogeneous model.

For each type of surface, the results corresponding to several values of k have been investigated. It was found that the influence of k is greater in the case of a noncatalytic surface than in the other two cases (Fig. 3). Moreover, comparisons between the nonequilibrium vibration computations and the equilibrium ones for values of $k = 0.01$ and 1 demonstrate that the influence of the vibrational nonequilibrium is visible only for an altitude between 95 and 65 km and only on a noncatalytic surface. On the ideal catalytic surface, the difference between the nonequilibrium vibration case and the equilibrium one is rather small. Thus, the more catalytic the surface, the less important the surface activity, regarding the coupling effects, because the diffusion part of the heat flux to the body surface increases with the catalytic activity.

In Fig. 4 the transrotational and vibrational temperatures (Fig. 4a) and the mass concentrations of the components (Fig. 4b) are plotted vs the dimensionless normal coordinate x^3/L: for an ideal catalytic surface, $H = 60$ km, $V_\infty = 4.75$ km/s and for two values of k. On the whole, the influence of the altitude on the transrotational and vibrational temperatures is rather great because the flow appears to be fully viscous ($Re = 300$) for an altitude of 80 km, whereas for $H = 60$ km, the flow is viscous just behind the shock wave and close to the body surface, but in between, the flow is inviscid. For both altitudes, the behavior near the shock wave depends on the coupling between the nonequilibrium phenomena and on the molecular transfer effects. Therefore, along the entire trajectory it is necessary to apply the generalized Rankine–Hugoniot relations to the shock wave. It can also be seen that even at an altitude of 60 km with $V_\infty = 4.75$ km/s and $L = 0.5$ m, the vibrational nonequilibrium effects are still great (for this trajectory): The temperature T resulting from a nonequilibrium computation is rather different from the one resulting from a vibrational equilibrium computation. This can be explained by the competitive influence of the Landau–Teller vibrational source term and of the vibration–chemistry coupling source term at an altitude of 60 km. The nonmonotonic behavior of $T_{V_{O_2}}$ is

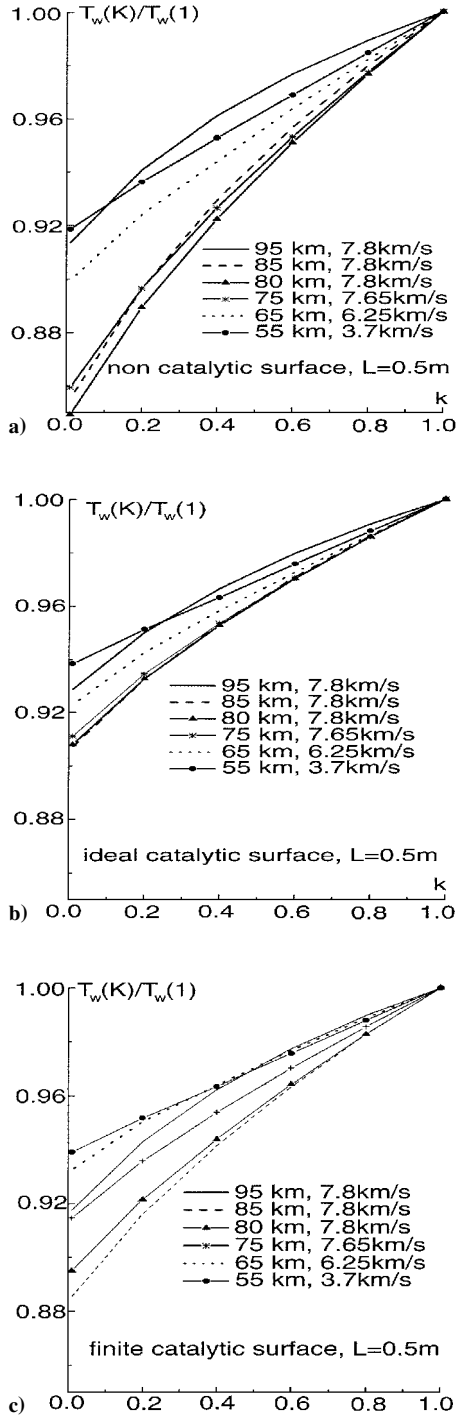

Fig. 5 Dependence of the ratio $T_w(k)/T_w(1)$ on k for different trajectory points and for different catalysis models; $L = 0.5$ m.

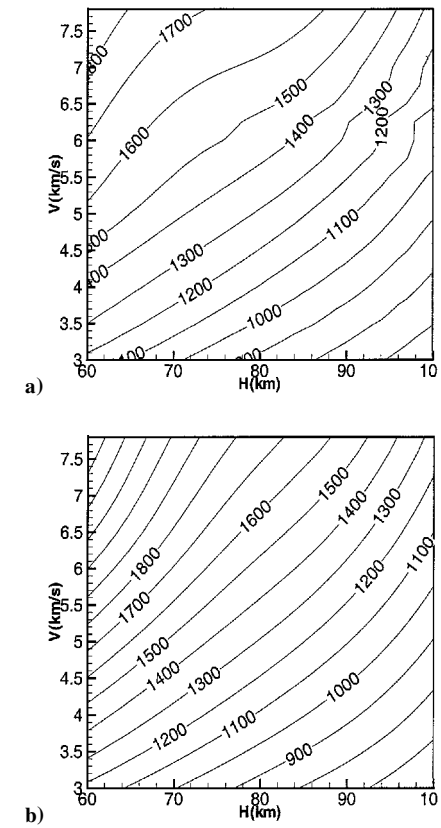

Fig. 6 Flow over a sphere, $L = 0.5$ m; isovalues of the wall equilibrium temperature $T_w(1)$ a) for a noncatalytic surface and b) for a finite catalytic surface.

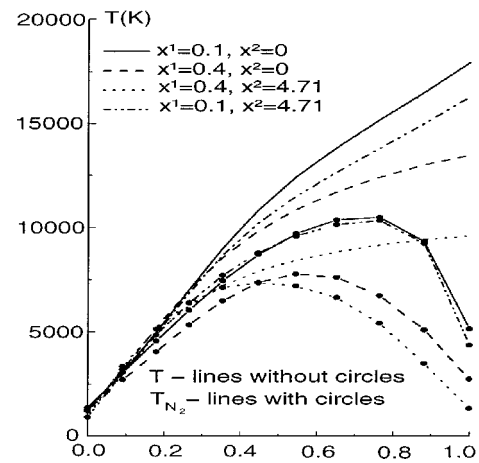

Fig. 7 Profiles of T and $T_{v_{N_2}}$ across the shock layer vs the coordinate ζ for different locations on the lateral ellipsoid surface.

particularly noteworthy as the altitude decreases. The local minima of the vibrational temperature of oxygen are for the altitudes of 90 and 60 km. This can be explained by the relatively low value of the Landau–Teller vibrational source term at a high altitude (90 km) and by the relatively low value of the temperature behind the shock wave at 60 km. However, whereas the behavior of $T_{V_{O_2}}$ is not monotonic with respect to the altitude, the difference between T and $T_{V_{O_2}}$ decreases monotonically as the altitude decreases.

The body shape and the surface catalysis also have a rather great influence on the levels of chemical components in the shock layer (Fig. 4b). Because the shock standoff distance for a flow around a sphere ($k = 1$) is shorter than for a small k, the ratio between the chemical relaxation characteristic timescale and the flow characteristic timescale increases; therefore, in the flow around the sphere, there is less dissociation of N_2 than in the flow around a body with a small k. As for the oxygen molecules, their full dissociation for $k = 1$ appears farther from the shock wave than for $k \sim 0.1$.

We have also investigated the dependence of the parameter $T_w(k)/T_w(1)$ on k, where $T_w(1)$ is the equilibrium wall temperature on a sphere, for different trajectory points and for different wall catalysis types (Fig. 5). This ratio seems to be quite conservative and has a similar behavior for different catalysis surfaces and for different freestream parameters.

As for the wall equilibrium temperature $T_w(1)$ for a flow over a sphere, its isovalues are drawn in Fig. 6a for a noncatalytic surface model and in Fig. 6b for the Tong et al. model.[16] These isovalues are determined for a range of altitude varying from 60 to 100 km and for a range of velocity varying from 3 to 7.8 km/s. These isovalues are very practical to use because, for any altitude and velocity, they allow the value of the wall temperature at the stagnation point of a flow over a sphere to be determined with a rather high accuracy. Then, knowing

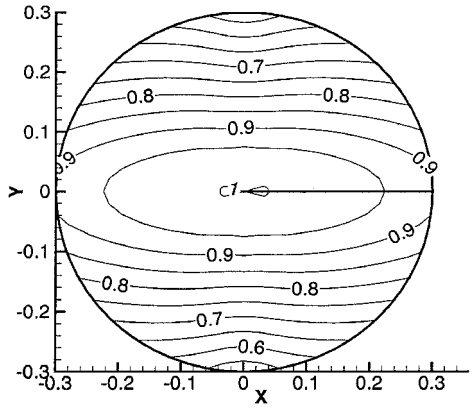

a) $\alpha = 0$ deg and $\beta = 0$ deg

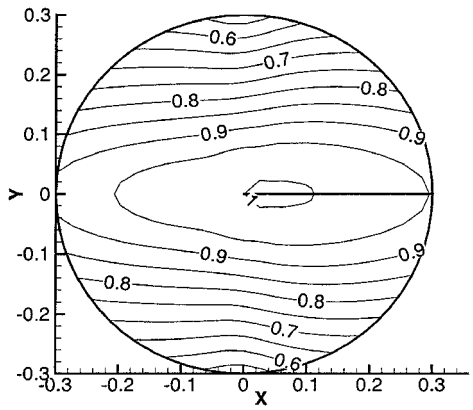

b) $\alpha = 20$ deg and $\beta = 0$ deg

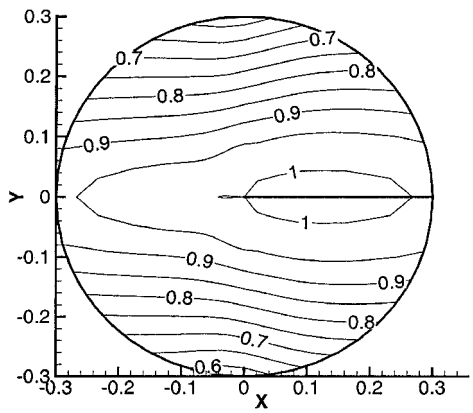

c) $\alpha = 45$ deg and $\beta = 0$ deg

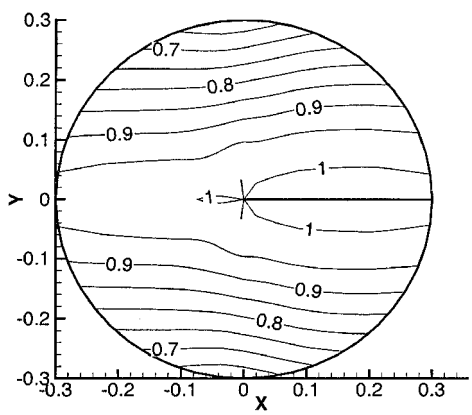

d) $\alpha = 60$ deg and $\beta = 0$ deg

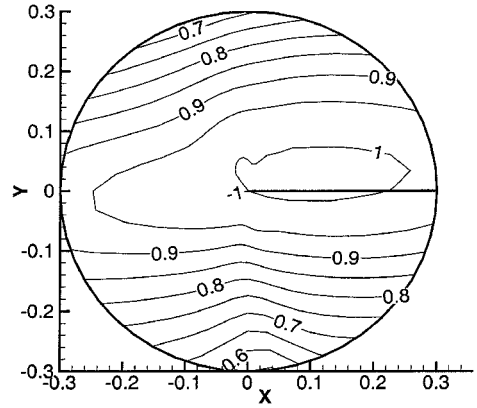

e) $\alpha = 45$ deg and $\beta = 15$ deg

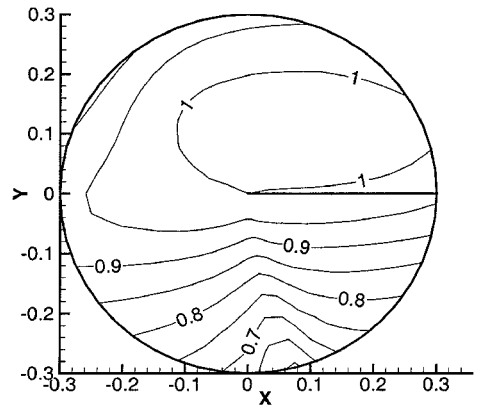

f) $\alpha = 45$ deg and $\beta = 45$ deg

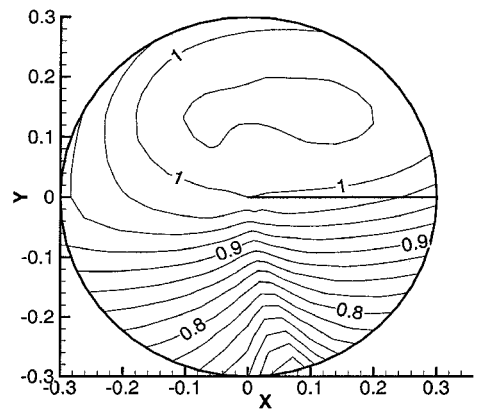

g) $\alpha = 45$ deg and $\beta = 60$ deg

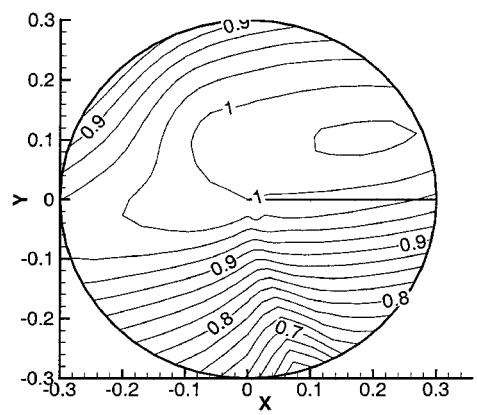

h) $\alpha = 60$ deg and $\beta = 30$ deg

Fig. 8 Flow over an ellipsoid with axis 1:0.7:0.3, $H = 70$ km, $V_\infty = 7.25$ km/s, and $L = 0.5$ m, where $x = x^1 \cos x^2$, $y = x^1 \sin x^2$; distributions of T_w^0 along a noncatalytic surface for different angles α and β.

$T_w(1)$ and using the conservatism of the ratio $T_w(k)/T_w(1)$ with respect to freestream parameters, the value of the wall temperature $T_w(k)$ can be determined for any other body shape by multiplying the value of $T_w(1)$ by the ratio $T_w(k)/T_w(1)$.

B. Three-Dimensional Flow over a Lateral Body Surface

Now consider the computational results for a general three-dimensional flow simulation. Figure 7 presents the profiles of the transrotational temperature T and of the vibrational temperature $T_{V_{N_2}}$ across the shock layer for different locations on the lateral ellipsoid surface (with axis 1:0.7:0.3, for the upstream conditions $H = 86.21$ km, $V_\infty = 7.25$ km/s, $L = 5.0$ m, and $\alpha = \beta = 45$ deg and for a noncatalytic surface).

The numerical simulation have demonstrated that the absolute values of the wall equilibrium temperature T_w and of the heat flux q_w strongly depend on the problem parameters (see Fig. 3), whereas the relative distributions of the q_w^0 and of the T_w^0 (referred to its values at the stagnation point) are more conservative, and for a number of cases T_w^0 and q_w^0 depend much less on H and V_∞ and on the catalytic reactions model.

The character of the T_w^0 distributions in a qualitative sense depends on the body shape and on the values of the angles α and β. Their influence on T_w^0 along the noncatalytic ellipsoid surface with axis 1:0.7:0.3 for $H = 70$ km, $V_\infty = 7.25$ km/s, and $L = 0.5$ m is presented in Fig. 8. For this ellipsoid, the distribution T_w^0 for $\alpha = \beta = 0$ deg has a maximum at the stagnation point. For nonzero incidence ($\alpha \neq 0$ deg) and $\beta = 0$ deg, the maximum of T_w^0 remains in a symmetry plane of the flow, but moves from the stagnation point to a direction of decrease in the longitudinal curvature radius of the ellipsoid. For a general case ($\alpha \neq 0$ deg and $\beta \neq 0$ deg) any symmetry for T_w^0 distributions disappears, and a limited region arises on the lateral surface of the body, where T_w exceeds its values at the stagnation point. On the whole, it has been found that a location of higher heat fluxes is defined by the values of the attack and slip angles and depends much less on the flight altitude.

The analysis of the numerical computations have also demonstrated that the relative values of the heat flux q_w^0 and of the equilibrium wall temperature T_w^0 are rather conservative with respect to the catalytic surface model, to the linear size of the problem L, and to the trajectory point. Indeed, this can be seen from the comparisons between T_w^0 isovalues for a noncatalytic surface (solid lines) and for a finite catalytic surface activity[16] (dashed lines) (Fig. 8a) and from the comparisons between T_w^0 distributions along a circumferential coordinate x^2 over the ellipsoid surface for different values of L (Fig. 9) ($H = 70$ km, $V_\infty = 7.25$ km/s, $\alpha = 45$ deg, and $\beta = 15$ deg).

For inviscid nonequilibrium airflow simulations the approximation of the binary similarity[33] has been widely practiced. The main idea of this approximation is that if recombination processes can be left out, the inviscid flow structure depends on the similarity parameter $B = \rho_\infty \cdot L$ only. In this connection, to verify the influence of recombination processes and of molecular transfer effects on the flow structure and the possibility to apply this approximate approach for the investigation of three-dimensional flows in viscous shock layers, a number of calculations have been carried out. An example of these comparisons is presented in Fig. 10, where the q_w^0 distributions along the marching coordinate x^1 are plotted for different altitudes and linear sizes (on condition that the similarity parameter $B = \rho_\infty \cdot L$ remains constant and equal to 2.95×10^{-5} kg/m^2), and for different catalysis models. Here lines a–e correspond to a noncatalytic surface; lines f–g to finite catalysis surface; lines a, e, and g to $H = 86.21$ km, and $L = 5.0$ m; lines and b, d, and f to $H = 53.78$ km, and $L = 0.05$ m; line c to $H = 70$ km and $L = 0.5$ m; and lines d and e to the vibrational equilibrium case. On the whole, comparisons with numerical solutions have demonstrated that the binary similarity approximation has rather good accuracy for the relative values of the heat flux q_w^0 and for the equilibrium wall temperature T_w^0, as well as for the absolute values of the heat transfer coefficient $C_q = 2q_w/(\rho_\infty V_\infty^3)$ distributions, and therefore, this approximation can be used for practical applications.

The conservative behavior of the equilibrium wall temperature relative value T_w^0 has an important practical significance because it allows the following approximate formula for the definition of the equilibrium surface temperature:

$$T_w\left(x^1, x^2, k, k_{iw}, L, \rho_\infty, V_\infty\right) = T_w(0, 0, k, k_{iw}, L, \rho_\infty, V_\infty) \times \bar{T}_w^0 \tag{23}$$

$T_w(0, 0, k, k_{iw}, L, \rho_\infty, V_\infty)$ can be defined by means of the numerical solution to the problem for the three-dimensional stagnation point with given values of the parameter k and of the problem linear size L, a given catalytic activity, and a given trajectory point. For the calculation of the term $\bar{T}_w^0$, the conservatism of the relative distributions T_w^0 can be used. On this basis, the value of $\bar{T}_w^0$ can be calculated only once for a given body shape and for given values of the angles α and β (for example for a noncatalytic surface and for one variant of the flight altitude and of the freestream velocity). Comparisons of numerical results and calculations with relation (23) are presented in Fig. 11, where the distributions T_w along the marching coordinate x^1 for a flow over an ellipsoid with axis 1:0.7:0.3 for $V_\infty = 7.25$ km/s and $\alpha = \beta = 45$ deg are plotted. In Fig. 11, lines 1 are for $H = 53.78$ km and $L = 0.05$ m; lines 2 for $H = 70$ km and $L = 0.5$ m with the vibrational equilibrium case; and lines 3 for $H = 86.21$ km and $L = 5.0$ m. As can be seen, the suggested approximate approach gives results close to the complete numerical results, and therefore, it may be used for practical applications.

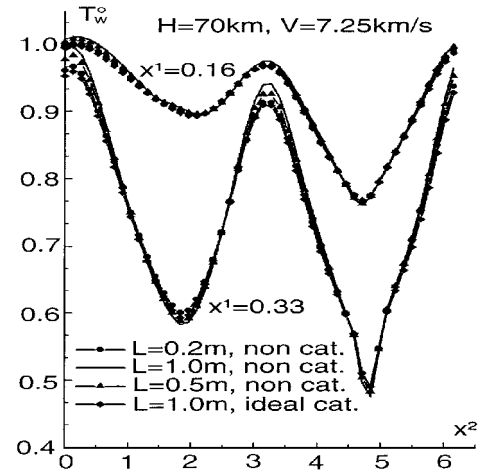

Fig. 9 Distributions of T_w^0 along the circumferential coordinate x^2 for different values of L; flow over an ellipsoid with axis 1:0.7:0.3, $\alpha = 45$ deg and $\beta = 15$ deg.

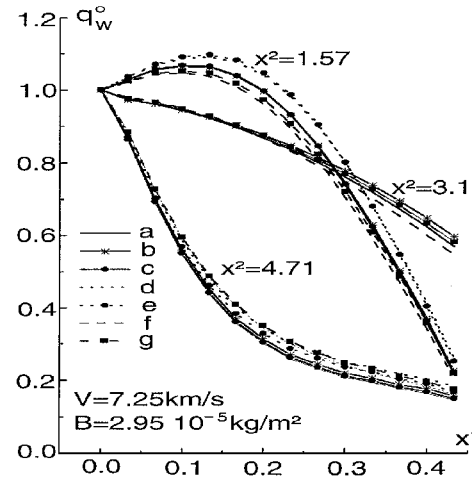

Fig. 10 Distributions of q_w^0 along the marching coordinate x^1 for different H and L; flow over an ellipsoid with axis 1:0.7:0.3, $\alpha = \beta = 45$ deg.

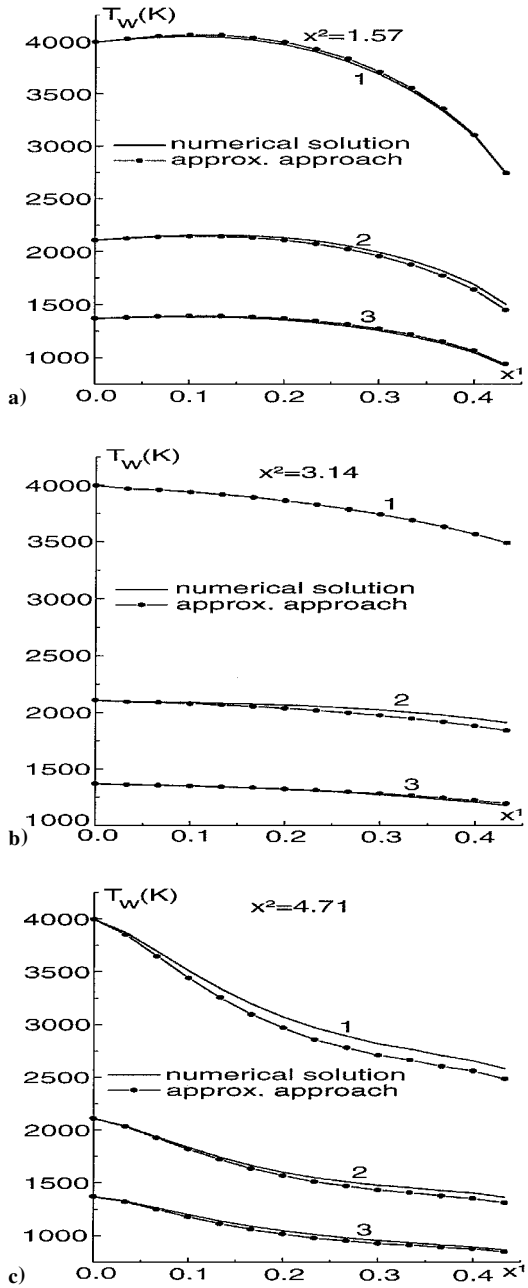

Fig. 11 Distributions of T_w(K) along the marching coordinate x^1; flow over an ellipsoid with axis 1:0.7:0.3, V_∞ = 7.25 km/s, and $\alpha = \beta = 45$ deg.

VI. Conclusions

The flowfield over a three axis ellipsoid for a wide range of freestream parameters and of attack and slip angles, including the practical application of the space shuttle trajectory, has been investigated. The determination of the three-dimensional flow parameters on the basis of the TVSL model has been carried out by taking into account the coupling between the vibrational relaxation and the chemical processes by means of the recently developed CVDEV model. The numerical simulations have been conducted with the high-accuracy numerical method, which has a very high level of arithmetic cost efficiency. It has been shown that the body surface heat flux and the equilibrium temperature strongly depend on the nonequilibrium coupling for a noncatalytic surface. For an ideal catalytic surface or for a finite catalytic surface, the influence of the coupling is lower, but to obtain accurate information about the structure of the shock layer, it is necessary to take into account the coupling for practically all of the trajectory and to consider viscous effects close to the shock wave. To conclude, the TVSL approach is a very powerful tool that has enabled the assessment of various assumptions about the modeling of reentry nonequilibrium flowfields.

Acknowledgments

This work was supported by the Université de Provence (Institut Universitaire des Systèmes Thermiques Industriels) and the Russian Fund of Fundamental Investigations (Project 98-01-00298).

References

[1]Hammerling, P., Teare, J. D., and Kivel, B., "Theory of Radiation from Luminous Shock Waves in Nitrogen," *Physics of Fluids*, Vol. 2, No. 4, 1959, pp. 422–426.

[2]Marrone, P., and Treanor, C., "Chemical Relaxation with Preferential Dissociation from Excited Vibrational Levels," *Physics of Fluids*, Vol. 6, No. 9, 1963, pp. 1215–1221.

[3]Park, C., "Assessment of Two-Temperature Kinetic Model for Dissociating and Weakly Ionizing Nitrogen," *Journal Thermophysics and Heat Transfer*, Vol. 2, No. 1, 1988, pp. 8–16.

[4]Macheret, S. O., Fridman, A. A., and El'kin, A. A., "Rates Constants of Exchange Reactions in Nonequilibrium Conditions: Classical Model," *Khimicheskaya Fizika (Soviet Chemical Physics)*, Vol. 9, No. 2, 1990, pp. 174–179.

[5]Zeitoun, D., Schall, E., Burtschell, Y., and Druguet, M.-C., "Vibration–Dissociation Coupling in Nonequilibrium Hypersonic Viscous Flows," *AIAA Journal*, Vol. 33, No. 1, 1995, pp. 79–85; also AIAA Paper 94-1989, June 1994.

[6]Knab, O., Fruhauf, H.-H., and Messerschmid, E. W., "Theory and Validation of the Physically Consistent Coupled Vibration–Chemistry–Vibration Model," *Journal of Thermophysics and Heat Transfer*, Vol. 9, No. 2, 1995, pp. 219–226.

[7]Bose, D., and Candler, G. V., "Kinetics of the $N_2 + O \rightarrow NO + N$ Reaction Under Thermodynamics Nonequilibrium," *Journal of Thermophysics and Heat Transfer*, Vol. 10, No. 1, 1996, pp. 148–154.

[8]Séror, S., Druguet, M.-C., Schall, E., and Zeitoun, D., "Coupled Vibration–Dissociation–Exchange Reactions Model for Hypersonic Airflow Computations," *AIAA Journal*, Vol. 36, No. 4, 1998, pp. 532–538; also AIAA Paper 97-2556, June 1997.

[9]Séror, S., Schall, E., Druguet, M.-C., and Zeitoun, D., "An Extension of CVDV Model to Zeldovich Exchange Reactions for Hypersonic Non-Equilibrium Air Flows," *Shock Waves*, Vol. 8, No. 5, 1998, pp. 285–298.

[10]Cheng, H. K., "Hypersonic Shock-Layer Theory of the Stagnation Region at Low Reynolds Number," *Proceedings of the Heat Transfer and Fluid Mechanic Institute*, Stanford Press, Stanford, CA, 1961, pp. 161–175.

[11]Gershbein, E. A., "Asymptotical Investigation of 3D Viscous Gas Flow Problem over Blunt Bodies with Permeable Surface," *Hypersonic 3D Flows with Physical–Chemical Effects*, Moscow Univ. Press, Moscow, 1981, pp. 29–51 (in Russian).

[12]Cherny, G. G., *Gas flow with Hypersonic Velocity*, Fizmatgiz, Moscow, 1959 (in Russian).

[13]Peigin, S. V., and Tirskii, G. A., "Super- and Hypersonic Three-Dimensional Viscous Flows," *Super- and Hypersonic Aerodynamics and Heat Transfer*, edited by G. K. Mikhailov and V. Z. Parton, CRC Press, London, 1993, pp. 91–202.

[14]Borodin, A. I., Kazakov, V. Y., and Peigin, S. V., "Multicomponent 3D Viscous Shock Layer Solutions for Blunt Bodies with a Catalytic Surface at Angles of Attack and Yaw," *Izvestiya Acad. Nauk, Mehan. Zhidkosti i Gasa*, No. 1, 1990, pp. 143–150 (in Russian).

[15]Peigin, S. V., "Numerical Simulation of 3D Hypersonic Reacting Flows over Blunt Bodies with Catalytic Surface," *Computational Methods in Applied Sciences*, Elsevier Science, Amsterdam, 1992, pp. 127–135.

[16]Tong, H., Buckingham, A. C., and Curry, D. M., "Computational Procedure for Evaluation of Space Shuttle TRS Requirements," AIAA Paper 74-518, 1974.

[17]Miner, E. W., and Lewis, C. H., "Hypersonic Ionizing Air Viscous Shock Layer Flows over Nonanalytic Blunt Bodies," NASA CR-2550, 1975.

[18]Wilke, C. R., "A Viscosity Equation Gas Mixtures," *Journal of Chemical Physics*, Vol. 18, No. 4, 1959, pp. 517–519.

[19]Mason, E. A., and Saxena, S. C., "Approximate Formula for the Thermal Conductivity," *Physics of Fluids*, Vol. 1, No. 5, 1958, pp. 361–368.

[20]Gurvich, L. V., Veic, I. A., and Medvedev, V. A., *Thermodynamic Property of Individual Substance*, Vol. 1, Book 2, Nauka, Moscow, 1978, p. 867.

[21]Landau, L., and Teller, E., "Theory of Sound Dispersion," *Physikalische Zeitschrift der Sowjetunion*, Vol. 34, No. 10, 1936, pp. 34–43.

[22]Millikan, R., and White, D., "Systematics of Vibrational Relaxation," *Journal of Chemical Physics*, Vol. 39, No. 12, 1963, pp. 3209–3213.

[23]Breshears, W. D., and Bird, P. F., "Effects of Oxygen Atoms on the Vibrational Relaxation of Nitrogen," *Journal of Chemical Physics*, Vol. 48, No. 10, 1968, p. 4773.

[24]Kiefer, J. H., and Lutz, R. W., "The Effects of Oxygen Atoms on the Vibrational Relaxation of Oxygen," *Proceedings of the 11th Symposium on Combustion*, Combustion Inst., Pittsburgh, PA, 1967, pp. 67–74.

[25]Petuhkov, I. V., "Numerical Solution of 2D Flows in Boundary Layer," *Numerical Methods of Differential and Integral Equations Solutions and Quadrature Formulas*, Nauka, Moscow, 1964, pp. 305–325.

[26]Masek, R. V., Hender, D., and Forney, J. A., "Evaluation of Aerodynamic Uncertainties for Space Shuttle," AIAA Paper 73-737, 1973.

[27]Séror, S., Zeitoun, D. E., Brazier, J.-P., and Schall, E., "Asymptotic Defect Boundary Layer Theory Applied to Thermochemical Non-Equilibrium Hypersonic Flows," *Journal of Fluid Mechanics*, Vol. 339, 1997, pp. 213–238.

[28]Séror, S., Schall, E., and Zeitoun, D. E., "Comparision Between Coupled Euler/Defect Boundary Layer and Navier–Stokes Solutions for Non-Equilibrium Hypersonic Flows," *Journal of Computers and Fluids*, Vol. 27, No. 3, 1998, pp. 381–406.

[29]Lobb, R. K., "Experimental Measurement of Shock Detachment Distance on Spheres Fired in Air at Hypervelocities," *Proceedings of the High Temperature Aspects of Hypersonic Flows*, edited by C. W. Nelson, Pergamon, New York, 1964, pp. 519–527.

[30]Brueck, S., "Hyperboloid Flare," *The Fourth European High Velocity Database Workshop*, European Space Research and Technology Center, Noordwijk, The Netherlands, 1994, Chap. 5.

[31]Fujiwara, T., and Aso, S., First US–European High Velocity Database Workshop, Rept. T12-95 OREX, Houston, TX, 1995.

[32]Vetter, M., Olivier, H., and Grönig, H., "Flow over Double Ellipsoid and Sphere—Experimental Results," *Hypersonic Flows for Reentry Problems*, Vol. 3, Springer, 1992, pp. 489–500.

[33]Gibson, W. E., "Dissociation Scaling for Nonequilibrium Blunt Nose Flows," *ARS Journal*, Vol. 32, No. 2, 1962.

M. Sichel
Associate Editor